JOURNAL OF THERMOPHYSICS AND HEAT TRANSFER
Vol. 13, No. 4, October–December 1999

Analysis of Molecular Gas Radiation: Real Gas Property Effects

K. C. Tang* and M. Q. Brewster†
University of Illinois at Urbana–Champaign, Urbana, Illinois 61801

Molecular gas radiation calculations have been performed for CO_2 and H_2O with a line-by-line high-resolution transmission molecular absorption database, with and without particle scattering. Both line-by-line (Monte Carlo) and *K*-distribution calculations were conducted. The results confirmed that, if the absorption-coefficient distribution function is sufficiently resolved, essentially line-by-line accuracy can be achieved. In addition, comparison was made between line-by-line results and an exponential wideband model combined with Elsasser narrowband model predictions to assess real gas property effects on radiative heat transfer. It was found that accurate prediction of the radiative heat flux and divergence requires a more accurate representation of the *K*-distribution than band model data currently provide. It was also found that the notion of an optically thin molecular gas based on the Planck mean optical thickness is probably a misleading concept. Analysis of real line-by-line data for typical thermodynamic conditions and path lengths suggests that in most practical systems at least some portion of a vibration-rotation band spectrum is optically thick. Hence, Planck mean optical thickness is an erroneous indicator of the validity of the Planck mean optically thin approximation for molecular gas radiation.

Nomenclature

f	= K-distribution function; Eq. (8)
h	= step function
I	= intensity
K or K_a	= absorption coefficient
K_e	= extinction coefficient
K_{em}	= emission coefficient
K_s	= scattering coefficient
L	= path length
N	= particle number density
P	= pressure
p	= scattering phase function
Q	= function defined by Eq. (5)
q	= radiative heat flux
T	= temperature
W	= slab width
x	= spatial coordinate
θ	= slab polar angle
μ	= direction cosine of considered polar angle $\theta(\mu = \cos\theta)$
μ'	= direction cosine of irradiation polar angle θ' or dummy argument

Subscripts

a	= absorption
b	= blackbody
c	= center
e	= extinction
eff	= effective
em	= emission
g	= gas
i	= species (gas, particles)
j	= dummy index
max, min	= local maximum and minimum values
P	= Planck mean
p	= particle
s	= scattering
ν	= wave number

Received 30 November 1998; revision received 14 May 1999; accepted for publication 14 May 1999.

*Research Programmer, Center for Simulation of Advanced Rockets; k-tang@uiuc.edu.

†Professor, Department of Mechanical and Industrial Engineering; brewster@uiuc.edu. Associate Fellow AIAA.

Introduction

THERE is a need for both exact and approximate property representations and transfer solution techniques in the calculation of radiation heat transfer. For gases, exact properties means line-by-line (LBL) or equivalent and approximate means band-model properties or low-order gray gas correlations. Exact transfer means Monte Carlo (MC) or high-order N-flux or discrete-ordinate (DO) methods with anisotropic multiple scattering; approximate transfer means low-order N-flux or DO, effective isotropic scattering, or effective nonscattering. There is room for improvement at all levels of approximation for both properties and transfer calculations.

In modeling of radiation heat transfer by molecular gases, band models with low spectral resolution have generally been considered acceptable. This assumption is partly due to expediency, as the calculation of high-resolution spectra for polyatomic molecules is significantly more complicated than that for diatomic or atomic species, and partly due to the fact that, historically, boundary flux has been the only reality check between experiments and calculations; detailed computational fluid dynamics (CFD) involving molecular gas radiative transfer (in which radiative flux divergence is important) is still lacking in physical validation. However, band-model approaches do not allow sufficient spectral resolution when accurate radiative flux divergence or distribution is required, when particle continuum radiation is present, or when severe temperature gradients exist. Moreover, even spectrally smoothed or integrated intensity at a boundary can be sensitive to fine line structure. There is no fundamental obstacle to modernizing engineering radiation heat transfer calculations to a high-spectral-resolution LBL model other than computer speed and storage and perhaps the absence of high-temperature and high-pressure data. However, brute-force LBL calculations are often unnecessarily time consuming. Pseudo-LBL treatment (LBL accuracy without LBL spectral integration) seems the next logical step in the development of radiation heat transfer simulation.

The K-distribution technique is a pseudo-LBL approach that was developed several decades ago by scientists studying atmospheric radiation.[1–4] Application of the K-distribution method to engineering systems has begun in recent years.[5–7] The basic idea of the technique is to take advantage of the fact that, although molecular

gas absorption-coefficient spectral fluctuations are severe, over the spectral region of a rotational–vibrational band particle properties and the Planck function are relatively constant with respect to wave number. Therefore, when the spectral distribution of the gas absorption coefficient is considered, the redundancy in brute-force spectral integration can be eliminated by integration with respect to absorption-coefficient distribution, i.e., the K distribution. Consequently, whereas spectral integration requires sufficient spectral resolution to resolve each line (of which there may be hundreds of thousands), K-distribution integration must resolve only the K distribution—a much more efficient computation. With K-distribution integration, essentially LBL accuracy is achievable with much less computational time.[6] If even lower computation time is desired this can be achieved by reduction of the resolution of the K distribution to a minimal number of discrete K values (say, three) with surprisingly little loss in accuracy, if the K's are chosen judiciously enough to cover the governing optical thicknesses. Our interest in this paper is with the former strategy, that is, maintaining exact LBL accuracy as nearly as possible. The objective of this work was to incorporate real gas LBL property data into the K-distribution technique and, by comparison with previous results based on band-model data, to assess the effect of real gas properties on radiation heat transfer. The LBL property data used were those of the high-resolution transmission molecular absorption (HITRAN) database.[8]

Solution Method

Radiative transfer is considered in a multicomponent, one-dimensional, nongray, emitting, absorbing, and scattering medium. Specifically the medium is composed of a participating molecular gas plus nonparticipating broadening gas and absorbing scattering particles. The radiative transfer equation is

$$\mu \frac{\mathrm{d}I_\nu(\mu)}{\mathrm{d}x} = -\sum_i \left(K_{s\nu_i} + K_{a\nu_i}\right) I_\nu(\mu) + \sum_i K_{\mathrm{em}\nu_i} I_{b\nu}(T_i) + \sum_i \frac{K_{s\nu_i}}{2} \int_{-1}^{1} I_\nu(\mu') p_i(\mu, \mu')\, \mathrm{d}\mu' \tag{1}$$

where I_ν is the spectral radiation intensity, ν is the wave number, T_i is the local temperature of species i, $I_{b\nu}$ is the spectral intensity of blackbody emission at T_i, $K_{a\nu_i}$, $K_{s\nu_i}$, and $K_{\mathrm{em}\nu_i}$ are the nongray absorption, scattering, and emission coefficients of species i, respectively, μ is the direction cosine of the polar angle measured from the x axis, $p_i(\mu, \mu')$ is the phase function of species i, which is a representation of intensity scattered from the incident radiation (direction μ') into the direction under consideration, μ. The spectral intensity can be obtained by solving the radiative transfer equation and associated boundary conditions. The net, spectral radiative heat flux can then be obtained by

$$q_\nu = 2\pi \int_{-1}^{1} I_\nu(\mu')\mu'\, \mathrm{d}\mu' \tag{2}$$

In LBL spectral integration Eq. (2) is evaluated with sufficient spectral resolution to resolve each line. The total radiative heat flux over the entire spectral region is then determined by integrating I_ν with respect to wave number:

$$q = \int_0^\infty q_\nu\, \mathrm{d}\nu = 2\pi \int_0^\infty \int_{-1}^{1} I_\nu(\mu')\mu'\, \mathrm{d}\mu'\, \mathrm{d}\nu \tag{3}$$

In the K-distribution approach the wave-number integration of Eq. (3) is transformed to an integration with respect to K_{a_g} as follows. Assuming that the Planck function and particle properties are constant within a band, the spectral intensity can be considered a function of the gas absorption coefficient only. Therefore the net flux for a gas band with bandwidth $\Delta\nu$ can be written as

$$q_{\Delta\nu} = \frac{1}{\Delta\nu} \int_{\Delta\nu} Q\left[K_{a_g}(\nu)\right] \mathrm{d}\nu \tag{4}$$

where

$$Q\left[K_{a_g}(\nu)\right] = 2\pi\,\Delta\nu \int_{-1}^{1} I_\nu\left[K_{a_g}(\nu), \mu'\right]\mu'\, \mathrm{d}\mu' \tag{5}$$

and the total radiative heat flux is obtained by summing over the bands:

$$q = \sum_{\text{all}\,\Delta\nu} q_{\Delta\nu} \tag{6}$$

By breaking up the lines into monotonic intervals $\mathrm{d}\nu_j$, summing over these intervals, and introducing the step function h, we can write Eq. (4) as[6]

$$\frac{1}{\Delta\nu} \int_{\Delta\nu} Q\left[K_{a_g}(\nu)\right] \mathrm{d}\nu = \int_0^\infty Q\left(K_{a_g}\right) f\left(K_{a_g}\right) \mathrm{d}K_{a_g} \tag{7}$$

where

$$f\left(K_{a_g}\right) = \sum_{j=1}^{N} \frac{1}{\Delta\nu} \left|\frac{\mathrm{d}\nu_j}{\mathrm{d}K_{a_g}}\right| \left[h\left(K_{a_g} - K_{a_g,\min^j}\right) - h\left(K_{a_g} - K_{a_g,\max^j}\right)\right] \tag{8}$$

Here $f(K_{a_g})$ is the absorption-coefficient distribution (or probability density) function. This function is obtained by standard statistical analysis of the gas absorption-coefficient spectra.

Integration of Eq. (7) requires discretization of K_{a_g} and $f(K_{a_g})$. Proper discretization is the key to success with this method. Improper discretization will produce erroneous results and confusing trends. Although greater refinement of the K distribution usually leads to improved accuracy, arbitrary refinement may not show noticeable improvement and can be easily mistaken for convergence, particularly if only the boundary flux is monitored. It has been shown that heat flux at the boundary alone is not a sufficient indicator of accuracy of the radiative transport representation.[9] It is therefore critically important that the discretization be guided by proper physical considerations. The proper physical parameter on which to base K-distribution discretization and refinement is optical thickness based on a representative path length, such as geometric-mean beam length.[10] (For a slab the geometric-mean beam length is twice the slab thickness.) Both the optically thin and the optically thick portions of the K distribution must be sufficiently resolved to represent accurately the net flux distribution and divergence field. The approach used here was to divide the cumulative distribution function into 10 equal intervals and to solve each interval separately. A bisection procedure was used to refine the distribution within each of the 10 intervals until convergence was achieved at each spatial location. This approach may appear to ignore path-length effect (i.e., optical depth) as it involves only the K distribution but with proper selection of the bandwidth $\Delta\nu$, proper distribution and discretization over optical depth is automatically achieved. Bandwidth was defined here by extending the wings of the band to wave numbers at which the optical depth was 0.2. (As a check of this assumption, if an optical depth of 0.1 is chosen as the cutoff, the gas radiation calculated by the synthetic band model contributes an additional maximum 5% radiative heat flux to the CO_2 bands for the lowest particle loading case with $N = 2.0 \times 10^7$ m^{-3} and 0.04% for the highest particle loading case with $N = 2.0 \times 10^9$ m^{-3}.) The maximum and the minimum K_a values as well as the bandwidths for each band are shown in Table 1. This treatment ensures that the important optically thin region is not excluded from the band. Thus proper resolution of each optical depth region is obtained along with an accurate representation of the integral in Eq. (7). The integration in Eq. (7) is independent of the method used to solve the radiative transfer equation. In this study, the transfer equation is solved with the method of DO with 20 ordinates. The intensity field for the spectral radiative transfer equation is calculated to converge to less than 1.0×10^{-7} relative error. The K distributions are obtained from statistical analysis of HITRAN data.[8] The total radiative heat flux for a gas absorption band is calculated to be within 1.0×10^{-3} relative

Table 1 Bandwidths and maximum and minimum absorption coefficients for CO_2 bands used in heat flux calculations; $P = 1$ atm, CO_2 mole fraction = 0.21, $T = 1000$ K

CO_2 band	2.0 μm	2.7 μm	4.3 μm	9.4 μm	10.4 μm	15 μm
ν_{min}, cm^{-1}	5125.0	3435.0	2065.0	1015.0	915.0	502.0
ν_{max}, cm^{-1}	5275.0	3885.0	2410.0	1105.0	1005.0	832.0
$K_{a_g,max}$,[a] cm^{-1}	1.1×10^{-3}	1.7×10^{-1}	9.4×10^{0}	6.9×10^{-3}	5.1×10^{-3}	1.5×10^{0}
$K_{a_g,max}$,[b] cm^{-1}	9.6×10^{-4}	8.8×10^{-2}	3.7×10^{0}	4.1×10^{-3}	7.2×10^{-3}	1.3×10^{0}
$K_{a_g,min}$,[a] cm^{-1}	7.2×10^{-9}	6.3×10^{-5}	8.1×10^{-5}	6.3×10^{-5}	3.4×10^{-5}	7.9×10^{-5}
$K_{a_g,min}$,[b] cm^{-1}	2.4×10^{-4}	1.4×10^{-4}	1.9×10^{-4}	1.4×10^{-4}	8.7×10^{-5}	6.2×10^{-5}

[a]HITRAN database used for gas properties. [b]Synthetic band model used for gas properties.

error after grid and K-distribution refinement. The total radiative heat flux for the entire spectrum has a relative error of 0.5%. Results for synthetic band-model data reported previously[6] were based on Edwards's exponential wideband model[11] and the Elsasser model for line structure[3] with an assumed line spacing of 1.0 cm^{-1}.

Problem Statement

A one-dimensional sample problem was selected to match the specifications of a round-robin test problem considered as part of a continuing symposium on solution methods for radiative heat transfer in participating media.[12] The geometry is an infinite parallel slab with cold and black boundaries containing a uniform mixture of carbon particles, CO_2, and N_2. The slab thickness is $W = 5$ m. The mixture temperature is 1000 K, and the total pressure is 1 atm. The CO_2 mole fraction is 0.21. The spherical carbon particle diameter is 30 μm, and the particle concentrations are $N = 2 \times 10^7$, 2×10^8, and 2×10^9 particles/m^3. The particle absorption and scattering cross sections were computed with Mie theory as described previously.[6] Gray, linear anisotropic scattering was assumed for the scattering phase function, with a linear anisotropic parameter of 0.65, which corresponds to moderate forward scattering (the strong forward-scattered diffraction component was removed from scattering consideration and treated as unscattered radiation). The particle absorption and scattering coefficients at 2.7 μm for $N = 2 \times 10^9$ m^{-3} were 0.014 and 0.015 cm^{-1}, respectively.

Real Gas Properties

HITRAN absorption-coefficient data for CO_2 are shown in Figs. 1 and 2 for the 2.7- and the 4.3-μm bands, respectively. These are the two strongest bands for the conditions under consideration. Additional bands for which calculations were made are 2.0, 9.4, 10.4, and 15.0 μm. These figures show the complicated line structure arising from a very large number of vibrational-rotational transitions. In contrast, Fig. 3 shows the synthetic wideband model data for the 2.7-μm band considered in our earlier paper.[6] The synthetic wideband model is a combination of Edwards's exponential wideband model and the Elsasser model to simulate the rapid change of the gas absorption coefficient as a function of wave number. What is striking is how little alike the synthetic and real data appear to be. Of course, it was never the purpose of wideband modeling to imitate even spectrally smoothed band structure (which is the domain of narrowband modeling), let alone fine line structure; the purpose of wideband modeling is primarily to represent the integrated emissivity [area under the curve $1 - \exp(-K_a L)$] for a wide range of temperatures, pressures, and path lengths. To do this requires not only that the integrated absorption coefficient (area under the curve K_a) be accurately represented, but that the distribution of absorption coefficient with respect to wave number also be accurately represented. In this regard Edwards's exponential wideband model has been remarkably successful, considering its simplicity. Nevertheless, a comparison of Figs. 1 and 3 shows that the combination of Edwards's exponential wideband model and the Elssaser model is still far from being able to sufficiently represent the rapid change in the gas absorption coefficient. Figures 4 and 5 show the probability distribution function of absorption coefficient (K distribution) for the 2.7-μm band (bin size 1.713×10^{-3} cm^{-1}) and the 4.3-μm band (bin size 9.39×10^{-2} cm^{-1}). The most probable absorption-coefficient values are seen to be the smaller values. It is evident

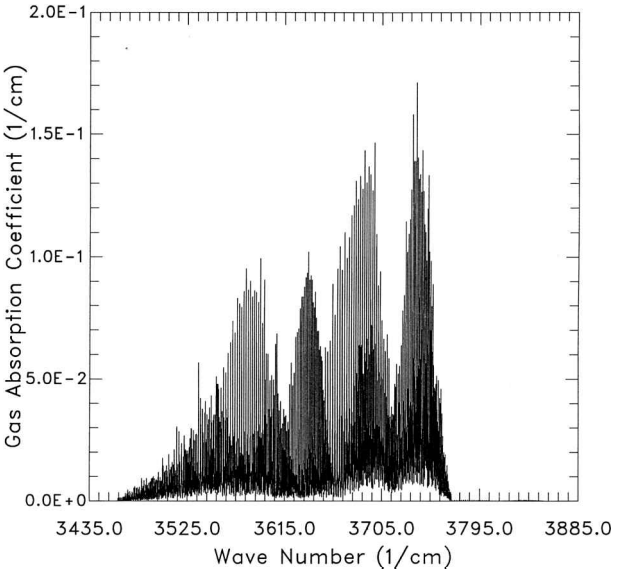

Fig. 1 HITRAN absorption coefficient for CO_2, 2.7-μm band, 21% (mole fraction) CO_2, and 79% N_2, 1000 K, 1 atm.

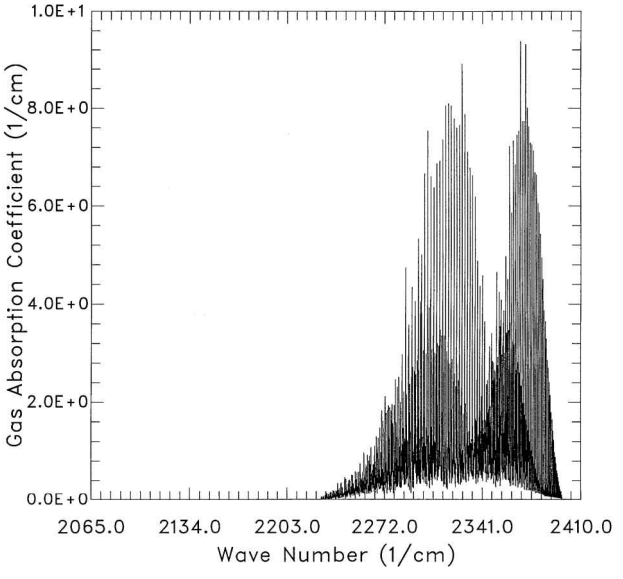

Fig. 2 HITRAN absorption coefficient for CO_2, 4.3-μm band, 21% (mole fraction) CO_2, and 79% N_2, 1000 K, 1 atm.

from Figs. 4 and 5 that the synthetic band model overestimates the K distribution for smaller absorption coefficients but underestimates the K distribution for the larger absorption coefficients compared with the HITRAN data for this case. Given its simplicity, the exponential wideband distribution is a surprisingly good representation of the real distribution (thanks to the Boltzmann distribution effect on rotational energy levels) for CO_2. Nevertheless, the discrepancy between the band representation and the LBL data is evident.

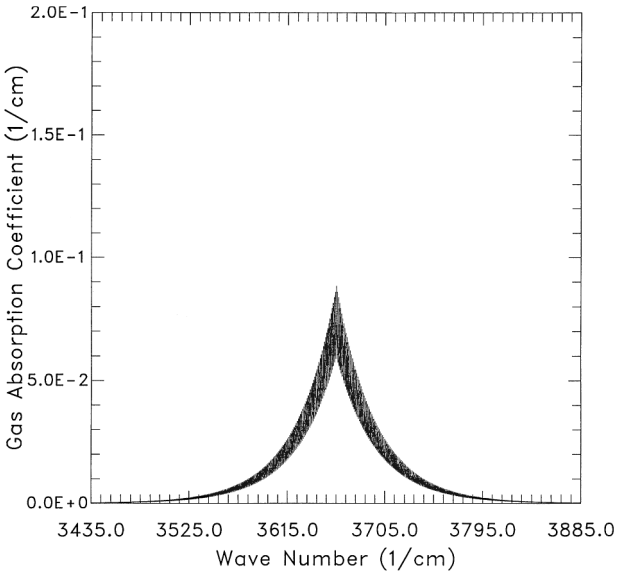

Fig. 3 Synthetic absorption coefficient for CO_2 (exponential wide-band/Elsasser), 2.7-μm band, 21% CO_2, 79% N_2, 1000 K, 1 atm.

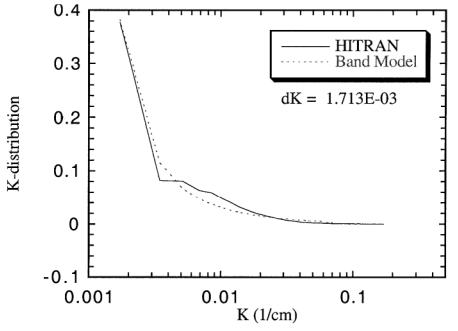

Fig. 4 K distribution for 2.7-μm band, 21% CO_2, 79% N_2, 1000 K, 1 atm.

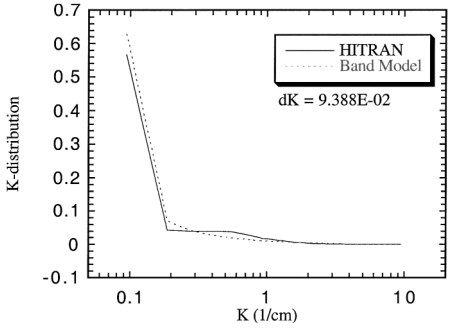

Fig. 5 K distribution for 4.3-μm band, 21% CO_2, 79% N_2, 1000 K, 1 atm.

Heat Transfer Results

Figure 6 shows the total, net radiant flux q vs spatial location x/W for both DO K-distribution calculations (DO) and Monte Carlo (MC) calculations. HITRAN properties were used for CO_2, and the results for three particle loadings are shown. The number of photons emitted in the MC calculations is increased until the relative error of the MC calculations is within 1%. The primary result of Fig. 6 is that the K-distribution approach gives essentially exact LBL accuracy. The results of K-distribution and MC calculations agree within 1%. A similar conclusion can be drawn for each CO_2 band. This result was reported earlier for the synthetic gas property data[6] and is confirmed here for the real gas property data. Figure 6

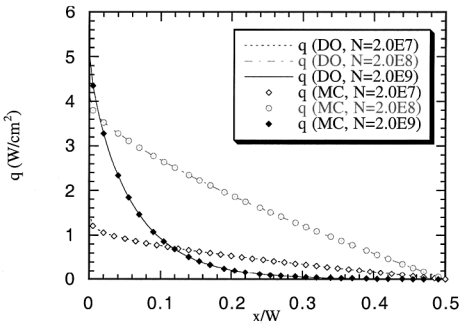

Fig. 6 Comparisons of total, net radiant heat flux distribution generated by DO method associated with K-distribution method and MC method by use of HITRAN database.

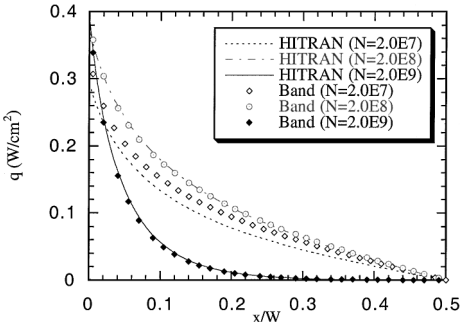

Fig. 7 Comparisons of 2.7-μm band net radiant heat flux distribution generated by HITRAN and by band model for isothermal slab, 5-m path length, 21% CO_2, 79% N_2, 1000 K, 1 atm, for three carbon particle loadings, N (number density given in inverse cubic meters).

also shows how the net flux varies with particle loading for this problem. Even for the lowest particle loading case ($N = 2 \times 10^7$), which has an approximate (2.7-μm) particle optical thickness of only $K_{e_p} L = 0.15$, particle radiation dominates that of the gas because of the relatively large spectral regions between gas bands. This case ($N = 2 \times 10^7$) shows a nearly linear increase in flux from zero at the center of the slab to the maximum value at the boundary. The intermediate particle loading case ($N = 2 \times 10^8$) shows an increase in flux over the previous case because of a higher particle optical depth ($K_{e_p} L = 1.5$) but still shows an essentially linear increase in flux with position over most of the slab. The highest particle loading case ($N = 2 \times 10^9$) shows a still higher flux at the boundary, as would be expected, but is also beginning to show the effects of a large particle optical thickness ($K_{e_p} L = 15$) by the decrease in flux in the slab interior and the nonlinear curvature of the flux distribution with x/W.

Figure 7 shows the radiant flux vs x/W for the 2.7-μm band obtained with both real gas HITRAN properties (K distribution) and band-model gas properties. For the highest particle loading ($N = 2 \times 10^9$) there is no distinguishable difference between the two property data sets used. This is because particle radiation is so strong for this case that any gas property differences are hidden. However, for the lowest particle loading ($N = 2 \times 10^7$), gas property differences are apparent by the deviation between the hollow diamond symbols and the dashed curve. These real gas property effects are even more apparent for the 4.3-μm band, as shown in Fig. 8. For the stronger 4.3-μm band, the difference between HITRAN and band-model gas properties is observable even for the highest particle loading case ($N = 2 \times 10^9$). It can be seen from Figs. 7 and 8 that the heat flux generated by HITRAN shows more nonlinear effect (because of the optically thick medium) than the heat flux generated by the band model. This is consistent with the fact from Figs. 4 and 5 that the K distribution generated by HITRAN had a higher distribution in the larger K_{a_g} region than the K distribution generated by the band model did. The error in flux is even more severe

Table 2 Band-by-band radiative heat flux (in watts per square centimeter) at boundary; $P = 1$ atm, CO_2 mole fraction = 0.21, $T = 1000$ K, $\delta = 1.0$ cm^{-1}

	$N = 2.0 \times 10^7$ m^{-3}		$N = 2.0 \times 10^8$ m^{-3}		$N = 2.0 \times 10^9$ m^{-3}	
CO_2 band	HITRAN[a]	Band[b]	HITRAN	Band	HITRAN	Band
2.0 μm	6.838×10^{-3}	1.902×10^{-2}	2.981×10^{-2}	3.355×10^{-2}	3.901×10^{-2}	3.916×10^{-2}
2.7 μm	2.933×10^{-1}	3.298×10^{-1}	3.729×10^{-1}	3.845×10^{-1}	3.899×10^{-1}	3.916×10^{-1}
4.3 μm	3.689×10^{-1}	5.218×10^{-1}	5.140×10^{-1}	5.670×10^{-1}	5.648×10^{-1}	5.729×10^{-1}
9.4 μm	4.981×10^{-2}	6.113×10^{-2}	8.717×10^{-2}	9.065×10^{-2}	9.829×10^{-2}	9.846×10^{-2}
10.4 μm	3.452×10^{-2}	4.987×10^{-2}	7.548×10^{-2}	8.003×10^{-2}	8.799×10^{-2}	8.826×10^{-2}
15.0 μm	1.813×10^{-1}	1.846×10^{-1}	2.096×10^{-1}	2.108×10^{-1}	2.106×10^{-1}	2.119×10^{-1}
Total	1.486	1.717	4.134	4.211	5.056	5.067

[a]HITRAN database used for gas properties. [b]Synthetic band model used for gas properties.

Table 3 Band-by-band divergence of radiative heat flux (in watts per cubic centimeter) at boundary, $W/8$, and $W/4$; $P = 1$ atm, CO_2 mole fraction = 0.21, $N = 2.0 \times 10^9$ m^{-3}, $T = 1000$ K, $\delta = 1.0$ cm^{-1}

	Boundary ($x = 0$)		$x = W/8$		$x = W/4$	
CO_2 band	HITRAN[a]	Band[b]	HITRAN	Band	HITRAN	Band
2.0 μm	1.402×10^{-3}	1.445×10^{-3}	1.701×10^{-4}	1.672×10^{-4}	3.054×10^{-5}	2.891×10^{-5}
2.7 μm	2.183×10^{-2}	2.404×10^{-2}	1.201×10^{-3}	1.136×10^{-3}	1.629×10^{-4}	1.544×10^{-4}
4.3 μm	3.222×10^{-1}	2.894×10^{-1}	1.131×10^{-3}	8.159×10^{-4}	1.785×10^{-4}	9.542×10^{-5}
9.4 μm	4.111×10^{-3}	4.167×10^{-3}	3.737×10^{-4}	3.697×10^{-4}	5.230×10^{-5}	5.070×10^{-5}
10.4 μm	3.676×10^{-3}	3.769×10^{-3}	3.347×10^{-4}	3.283×10^{-4}	4.674×10^{-5}	4.442×10^{-5}
15.0 μm	2.356×10^{-2}	3.458×10^{-2}	4.112×10^{-4}	3.884×10^{-4}	4.120×10^{-5}	3.822×10^{-5}

[a]HITRAN database used for gas properties. [b]Synthetic band model used for gas properties.

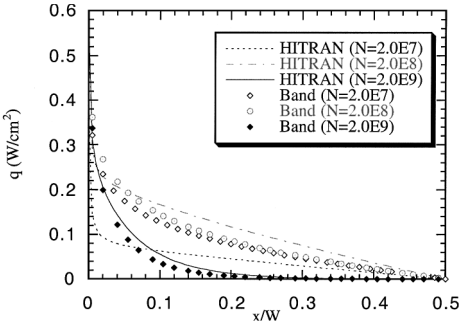

Fig. 8 Comparisons of 4.3-μm band net radiant heat flux distribution generated by HITRAN and by band model for isothermal slab, 5-m path length, 21% CO_2, 79% N_2, 1000 K, 1 atm, for three carbon particle loadings, N (number density given in inverse cubic meters).

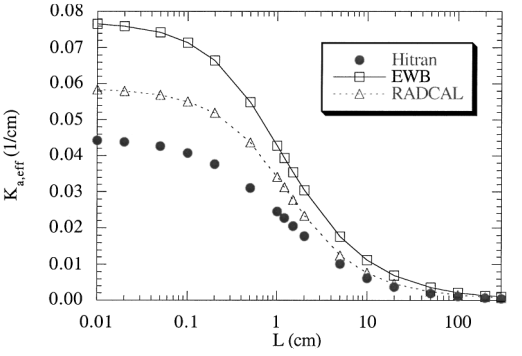

Fig. 9 Effective absorption coefficient for 21% CO_2, 79% N_2, 1000 K, 1 atm.

for the lower particle loading cases. It should be noted that these errors in net flux are significant and translate into substantial error in the radiative flux divergence. Thus, although in some cases (e.g. 4.3-μm band with $N = 2.0 \times 10^9$ m^{-3}) the boundary flux error may not be serious, as can be seen in the summary of boundary fluxes in Table 2, the radiative flux divergence (Table 3), which is important as a coupling source term in the energy equation, can exhibit significant error (>10%) because of inadequate representation of the real gas properties. One need only imagine a situation with negligible particle radiation contribution to appreciate the significance of these findings. In the following section, particle radiation is neglected and the effect of real gas properties in a pure, nonscattering, molecular gas is considered.

Pure Gas Radiation

In this section the emission and absorption properties of CO_2 and H_2O are considered for the same thermodynamic conditions as those in the previous section (1000 K, 1-atm total pressure, 0.21 mole fraction of emitting gas, N_2 broadening) and additional temperatures. A comparison among HITRAN,[8] exponential wideband,[11] and radiation calculation (RADCAL) narrowband[13] model data is made on the basis of the effective mean absorption coefficient for an isothermal, homogeneous path of length L, as defined in[14]

$$K_{a,\text{eff}} = \frac{\int_{\Delta\nu} K_a I_{b_\nu} \exp(-K_a L)\, \mathrm{d}\nu}{\int_{\Delta\nu} I_{b_\nu} \exp(-K_a L)\, \mathrm{d}\nu} \tag{9}$$

Based on this definition, the emissivity for a path length L is

$$\varepsilon = 1 - \exp(-K_{a,\text{eff}} L) \tag{10}$$

Figures 9 and 10 show $K_{a,\text{eff}}$ as a function of path length for CO_2 and H_2O, respectively, at 1000 K for all bands (the entire spectral region). HITRAN, RADCAL narrowband, and exponential wideband results are shown. The value of $\mathrm{d}\nu$ is bisected until the integration terms in Eq. (9) converge to less than 0.1% error. In the limit $L \to 0$, the effective absorption coefficient approaches the Planck mean value, $K_{a,P}$. In the limit $L \to \infty$, the effective absorption coefficient approaches the minimum value of K_a over the interval $\Delta\nu$. As discussed earlier with regard to band limits, the bandwidth $\Delta\nu$ should be extended to be wide enough to cover all of the important optically thin region such that assuming that $K_a = 0$ outside of $\Delta\nu$ does not introduce appreciable error. Thus, if optical thickness of 0.1 was judged to be sufficiently small, the minimum value of K_a should be of the order

Table 4 Maximum absorption coefficients for CO_2 bands used in computing the data points of Fig. 9; $P = 1$ atm, CO_2 mole fraction = 0.21, $T = 1000$ K

CO_2 band	2.0 μm	2.7 μm	4.3 μm	9.4 μm	10.4 μm	15 μm
$K_{a_g,\max}$,[a] cm^{-1}	1.1×10^{-3}	1.7×10^{-1}	9.4×10^{0}	6.9×10^{-3}	5.1×10^{-3}	1.5×10^{0}
$K_{a_g,\max}$,[b] cm^{-1}	9.5×10^{-4}	7.3×10^{-2}	3.5×10^{0}	3.0×10^{-3}	2.6×10^{-3}	5.3×10^{-1}
$K_{a_g,\max}$,[c] cm^{-1}	3.6×10^{-4}	5.2×10^{-2}	1.9×10^{0}	3.8×10^{-3}	1.6×10^{-3}	3.3×10^{-1}

[a]HITRAN database used for gas properties. [b]Edwards's wideband model used for gas properties. [c]RADCAL narrowband model used for gas properties.

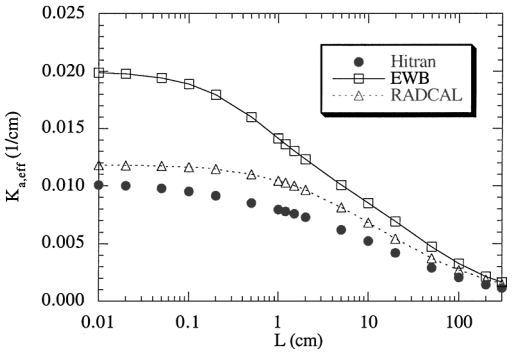

Fig. 10 Effective absorption coefficient for 21% H_2O, 79% N_2, 1000 K, 1 atm.

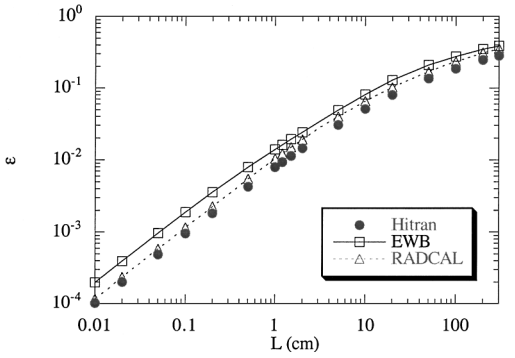

Fig. 12 Total emissivity for 21% H_2O, 79% N_2, 1000 K, 1 atm.

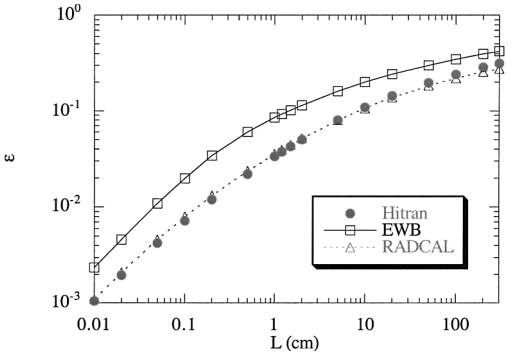

Fig. 11 Total emissivity for 21% H_2O, 79% N_2, 296 K, 1 atm.

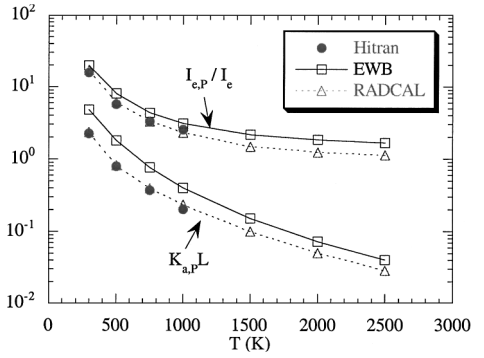

Fig. 13 Ratio of Planck intensity to actual intensity and Planck mean optical thickness for 21% H_2O, 79% N_2, 1 atm, $L = 20$ cm.

of $0.1/L$, which indicates that in the limit $L \to \infty$, the minimum value of K_a and hence the effective absorption coefficient approach zero. In the present calculations the intervals were taken to be zero to infinity and the minimum value of K_a was essentially zero. The maximum K_a values used in computing the data points of Fig. 9 are shown in Table 4. As can be seen in Figs. 9 and 10 there is a noticeable discrepancy between the real gas HITRAN data and the exponential wideband model data. The error in $K_{a,\text{eff}}$ is as large as 100% in the optically thin limit. This error carries over into the total emissivity calculated from Eq. (10), which is plotted in Figs. 11 and 12 for H_2O at 296 and 1000 K, respectively. In the optically thin limit the total emissivity for H_2O (Figs. 11 and 12) is overpredicted by a factor of 2 for the exponential wideband model.

The reason for the discrepancies seen in Figs. 9–12 is the error in the K_a distributions used by band models. Band models generally underrepresent the percentage of higher K_a values and overrepresent the percentage of lower ones, as illustrated in Figs. 4 and 5. As a result, at short path lengths, $K_{a,\text{eff}}$ and total emissivity are consistently overpredicted by band models. What the HITRAN data thus show (that band-model data do not) is that for most practical system configurations (typical thermodynamic conditions and path lengths) there will always be at least some optically thick portion of the spectrum. The assumption that all lines are optically thin is valid for only very short path lengths.

In this regard it is important to note that the criterion for determining applicability of the Planck mean optically thin limit is still frequently misunderstood in the literature as being $K_{a,P}L \ll 1$. Consideration of a real molecular gas line structure shows that it is quite possible to have a significant portion of the spectrum (i.e., line centers) be optically thick, while a significant portion (between lines) is optically thin, such that the condition $K_{a,P}L \ll 1$ would indeed hold but the Planck mean prediction would fail badly. That is, in the optically thick lines ($K_aL \gg 1$) the emitted spectral intensity along an isothermal path would be $[1 - \exp(-K_aL)]I_{b_\nu} \ll K_aLI_{b_\nu}$ such that the accuracy of the Planck mean value as an effective emission (or absorption) coefficient would be greatly reduced. This effect can be seen in Figs. 9 and 10. If $K_{a,P}L < 0.2$ was taken as the criterion of Plank mean applicability, Fig. 10 for H_2O, which gives $K_{a,P} = 0.010$ cm^{-1}, shows that the limiting path length would be ~20 cm. At this value of L the Planck mean value ($0.010\,cm^{-1}$) overestimates the actual effective absorption coefficient ($0.004\,cm^{-1}$) by a factor of 2.5. The emitted intensity would also be overpredicted by approximately this amount. This degree of error is quite large given the relatively small value of the Planck mean absorption coefficient ($K_{a,P}L = 0.2$).

Figure 13 shows the ratio of Planck predicted to actual intensity for the case just considered (1000 K, $L = 20$ cm) as well as for other temperatures. The error decreases with increasing temperature, primarily because of to the decreasing concentration of H_2O; nevertheless a factor of approximately 2 error in $I_{e,P}/I_e$ exists at temperatures as high as 2000 K, at which the Planck mean optical thickness is even smaller ($K_{a,P}\,L = 0.07$) for the exponential wideband model.

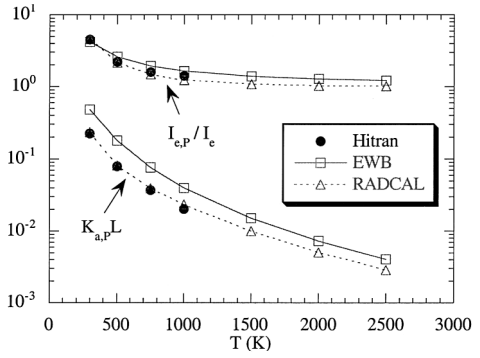

Fig. 14 Ratio of Planck intensity to actual intensity and Planck mean optical thickness for 21% H_2O, 79% N_2, 1 atm, $L = 2$ cm.

Figure 14 shows a similar plot for a 2 cm path length. At 300 K the Planck mean optical thickness is $K_{a,P}L = 0.2$, suggesting an error of only 20% associated with the Planck mean approximation, when in reality the error in emitted intensity is over 350% (a factor of 4.5) as shown in Fig. 14 for the HITRAN calculation. Similar conclusions can be drawn for the RADCAL narrowband and exponential wideband model calculations. Another comparison that can be made is between the HITRAN and RADCAL narrowband or exponential wideband results. It can be seen in Figs. 9–14 that the discrepancy between the HITRAN and the RADCAL results is generally less than that between HITRAN and wideband results. In Figs. 13 and 14, the HITRAN data points for higher temperatures are not available. To extend the applicability of HITRAN to higher temperatures, the addition of hot bands and high-temperature correlation are necessary. The results of Figs. 13 and 14 show how important it is to investigate thoroughly the conditions for applying the Planck mean optically thin approximation for the cases of real gas radiation with severe nongray effects and not simply rely on the Planck mean optical thickness.

Conclusion

Detailed molecular gas radiation calculations have been performed for CO_2 and H_2O with the LBL HITRAN database, with and without particle scattering. Both exact LBL (MC) and K-distribution calculations were conducted. The results showed that, if the absorption-coefficient distribution function (K distribution) was sufficiently resolved, essentially exact LBL accuracy was achieved with a significant reduction in computation time. Comparison of exact LBL results was also made with exponential wideband model predictions to assess real gas property effects. There is significant difference in radiative flux between HITRAN and band-model results, especially in the cases of low particle loading. For some particular conditions, band-model treatment may appear adequate in predicting radiative heat flux at boundaries, given an accurate temperature distribution. However, in terms of the spatial distribution of the net radiative flux in the gas (i.e., divergence of the radiative flux vector), band-model data can introduce significant errors even when the boundary flux appears to be correct. This is important particularly in situations in which the temperature field is not known and is to be predicted as part of a CFD calculation coupled with the radiative transfer. In such situations an accurate representation of the radiative flux divergence is critical, and LBL or pseudo-LBL treatment of K distribution must be considered. For pure gas systems, the error introduced by approximate gas radiation property data (exponential wideband model) is more significant. Under optically thin conditions, wideband model data overpredict effective absorption coefficient and total emissivity by approximately a factor of 2, at temperatures of 296–1000 K and atmospheric pressure, compared with HITRAN data. The discrepancy between HITRAN and RADCAL results appears to be less than that between HITRAN and wideband results.

Acknowledgments

Support for this work from the University of Illinois Research Board and computer time provided by the National Center for Supercomputing Applications at the University of Illinois at Urbana–Champaign is gratefully acknowledged. Research funded by the U.S. Department of Energy through the University of California under subcontract number B341494 is also gratefully acknowledged.

References

[1]Arking, A., and Grossman, K., "The Influence of Line Shape and Band Structure on Temperatures in Planetary Atmospheres," *Journal of Atmospheric Sciences*, Vol. 29, No. 5, 1972, pp. 937–949.

[2]Domoto, G. A., "Frequency Integration for Radiative Transfer Problems Involving Homogeneous Non-Gray Gases: The Inverse Transmission Function," *Journal of Quantitative Spectroscopy and Radiative Transfer*, Vol. 14, No. 9, 1974, pp. 935–942.

[3]Goody, R. M., and Yung, Y. L., *Atmospheric Radiation Theoretical Basis*, 2nd ed., Oxford Univ. Press, New York, 1989, p. 169.

[4]Goody, R., West, R., Chen, L., and Crisp, D., "The Correlated-K Method for Radiation Calculations in Nonhomogeneous Atmospheres," *Journal of Quantitative Spectroscopy and Radiative Transfer*, Vol. 42, No. 6, 1989, pp. 539–550.

[5]Tang, K. C., and Brewster, M. Q., "K-Distribution Analysis of Gas Radiation with Non-Gray, Emitting, Absorbing, and Anisotropic Scattering Particles," *28th National Heat Transfer Conference, Proceedings of Symposium on Solution Methods for Radiative Transfer in Participating Media*, ASME HTD-Vol. 203, American Society of Mechanical Engineers, New York, 1992, pp. 311–320.

[6]Tang, K. C., and Brewster, M. Q., "K-Distribution Analysis of Gas Radiation with Nongray, Emitting, Absorbing, and Anisotropic Scattering Particles," *Journal of Heat Transfer*, Vol. 116, No. 4, 1994, pp. 980–985.

[7]Marin, O., and Buckius, R. O., "Wideband Correlated-k Method Applied to Absorbing, Emitting, and Scattering Media," *Journal of Thermophysics and Heat Transfer*, Vol. 10, No. 2, 1996, pp. 364–371.

[8]Rothman, L. S., Gamache, R. R., Tipping, R. H., Rinsland, C. P., Smith, M. A. H., Benner, D. Chris, Devi, V. Malathy, Flaud, J.-M., Camy-Peyret, C., Perrin, A., Goldman, A., Massie, S. T., Brown, L. R., and Toth, R. A., "The HITRAN Molecular Database: Editions of 1991 and 1992," *Journal of Quantitative Spectroscopy and Radiative Transfer*, Vol. 48, No. 5/6, 1992, pp. 469–508.

[9]Kim, T. K., Menart, J. A., and Lee, H. S., "Nongray Radiative Gas Analyses Using the S-N Discrete Ordinates Method," *Journal of Heat Transfer*, Vol. 113, No. 4, 1991, pp. 946–951.

[10]Brewster, M. Q., *Thermal Radiative Transfer and Properties*, Wiley, New York, 1992, p. 349.

[11]Edwards, D. K., and Balakrishnan, A., "Thermal Radiation by Combustion Gases," *International Journal of Heat and Mass Transfer*, Vol. 16, No. 1, 1973, pp. 25–40.

[12]Tong, T. W., and Skocypec, R. D., "Summary on Comparison of Radiative Heat Transfer Solutions for a Specified Problem," *28th National Heat Transfer Conference, Proceedings of Symposium on Solution Methods for Radiative Transfer in Participating Media*, ASME HTD-Vol. 203, American Society of Mechanical Engineers, New York, 1992, pp. 253–258.

[13]Grosshandler, W. L., "RADCAL: A Narrow Band Model for Radiation Calculations in a Combustion Environment," National Inst. of Standards and Technology, NIST TN 1402, Gaithersburg, MD, April 1993.

[14]Patch, R. W., "Effective Absorption Coefficients for Radiant Energy Transport in Nongrey, Nonscattering Gases," *Journal of Quantitative Spectroscopy and Radiative Transfer*, Vol. 7, No. 4, 1967, pp. 611–637.